

# A Robotic Ultrasound Scanner for Automatic Vessel Tracking and Three-Dimensional Reconstruction of B-Mode Images

Samir Merouche, Louise Allard, Emmanuel Montagnon, Gilles Soulez, Pascal Bigras,  
and Guy Cloutier, *Senior Member, IEEE*

**Abstract**—Locating and evaluating the length and severity of a stenosis is very important for planning adequate treatment of peripheral arterial disease (PAD). Conventional ultrasound (US) examination cannot provide maps of entire lower limb arteries in 3-D. We propose a prototype 3D-US robotic system with B-mode images, which is nonionizing, noninvasive, and is able to track and reconstruct a continuous segment of the lower limb arterial tree between the groin and the knee. From an initialized cross-sectional view of the vessel, automatic tracking was conducted followed by 3D-US reconstructions evaluated using Hausdorff distance, cross-sectional area, and stenosis severity in comparison with 3-D reconstructions with computed tomography angiography (CTA). A mean Hausdorff distance of  $0.97 \pm 0.46$  mm was found *in vitro* for 3D-US compared with 3D-CTA vessel representations. To evaluate the stenosis severity *in vitro*, 3D-US reconstructions gave errors of 3%–6% when compared with designed dimensions of the phantom, which are comparable to 3D-CTA reconstructions, with 4%–13% errors. The *in vivo* system's feasibility to reconstruct a normal femoral artery segment of a volunteer was also investigated. These results encourage further ergonomic developments to increase the robot's capacity to represent lower limb vessels in the clinical context.

**Index Terms**—Image reconstruction, medical robotics, robotics and automation, ultrasonic imaging, ultrasonography.

Manuscript received January 17, 2014; accepted November 5, 2015. Date of publication November 9, 2015; date of current version December 29, 2015. This work was supported by the Fonds Québécois de la Recherche sur la Nature et les Technologies (FQRNT) under Grant PR-138400.

S. Merouche and E. Montagnon are with the Laboratory of Biorheology and Medical Ultrasonics, Research Center of the University of Montreal Hospital (CRCHUM), Montréal, QC H2X 0A9, Canada, and also with the Institute of Biomedical Engineering, University of Montreal, Montréal, QC H3T 1J4, Canada.

L. Allard is with the Laboratory of Biorheology and Medical Ultrasonics, Research Center of the University of Montreal Hospital (CRCHUM), Montréal, QC H2X 0A9, Canada.

G. Soulez is with the Institute of Biomedical Engineering, University of Montreal, Montréal, QC H3T 1J4, Canada, also with the Department of Radiology, University of Montreal Hospital (CHUM), Montréal, QC H2L 4M1, Canada, and also with the Department of Radiology, Radio-Oncology and Nuclear Medicine, University of Montreal, Montréal, QC H3T 1J4, Canada.

P. Bigras is with the Department of Automated Manufacturing Engineering, École de Technologie Supérieure, University of Quebec, Montréal, QC H3C 1K3, Canada.

G. Cloutier is with the Laboratory of Biorheology and Medical Ultrasonics, Research Center of the University of Montreal Hospital (CRCHUM), Montréal, QC H2X 0A9, Canada, with the Institute of Biomedical Engineering, University of Montreal, Montréal, QC H3T 1J4, Canada, and also with the Department of Radiology, Radio-Oncology and Nuclear Medicine, University of Montreal, Montréal, QC H3T 1J4, Canada (e-mail: guy.cloutier@umontreal.ca).

Digital Object Identifier 10.1109/TUFFC.2015.2499084

## I. INTRODUCTION

**T**O PLAN surgery or endovascular interventions, an overview of the lower limb arterial tree is required to determine the extent of peripheral arterial disease (PAD) and to locate and quantify the most severe proximal stenosis potentially affecting downstream hemodynamic and tissue perfusion. Physicians rely on digital subtraction angiography (DSA), computed tomography angiography (CTA), or magnetic resonance angiography (MRA) to get this clinical information. DSA offers a high performance to evaluate the severity of arterial stenoses but it is invasive and has a high risk of complication. CTA and contrast-enhanced MRA present a high accuracy for detecting and assessing significant stenoses greater than 50%, with reported sensitivities between 89% and 99% and specificities between 83% and 97% [1]. However, although CTA is a minimally invasive imaging method, patients that have to undergo multiple exams during their lifetime can be exposed to a significant risk due to ionizing radiation. Otherwise, MRA tends to underestimate the stenosis severity [1], its access remains limited and some patients do not tolerate being restricted in the tight bore of the instrument.

Ultrasound (US) imaging is the primary noninvasive means for PAD diagnosis and follow-up. The clinical literature reports that femoral artery duplex US diagnosis gives sensitivity of 80%–98% and specificity of 89%–99% to detect stenoses greater than 50%. Even though Doppler US has the best cost-effectiveness [1], it does not allow mapping the architecture of lower limb arteries, and tandem stenoses affect the diagnosis [2]. Over the years, 3D-US imaging has become widespread, now competing with conventional 2D-US imaging in obstetrics, peripheral vascular evaluation, and echocardiography [3]–[5]. Clinical studies with external 3D-US scanning have shown that this modality is able to characterize and quantify stenoses noninvasively in carotid arteries [6]–[9] and the 3-D geometry of the anastomosis in peripheral lower limb arteries [10]. However, most of these systems rely on a positioning tracking device and can only scan short segments. Therefore, they are not optimum for the examination of lower limb arteries, due to the restricted range of the probe motion detection, electromagnetic signal interference, or tracking visibility [11]–[13].

To provide accurate 3D-US scanning of lower limb vessels, an US robotic system was designed by our team [14]. The system has two operating modes. First, a teaching mode enables the learning of a “freehand” scan coupled with a replay mode

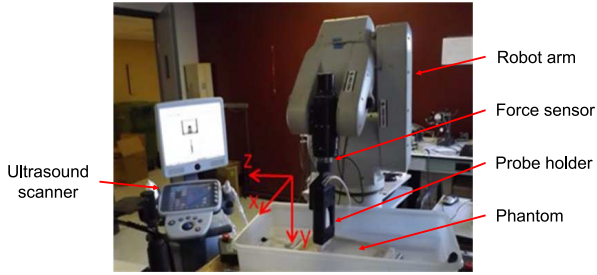


Fig. 1. Experimental setup. Overview of the 3D-US robotic system prototype scanning a vascular phantom. The  $x$ ,  $y$ ,  $z$  coordinate system corresponds to the base of the robot (i.e., robot CRS).

to reproduce the manually taught path. The scanning system captures and stores US images with their registered 3-D spatial locations at uniform spacing in replay mode. In the free command development mode, the US robotic system allows the implementation of customized programs to control the robot's movements. The accuracy of 2D-US image coordinates in the robot reference system was demonstrated by a calibration procedure with a  $Z$ -fiducial phantom [15].

In this study, we did not use the teach/replay mode of the previous design because for clinical applications, this concept may be limited by movement artifacts between teach and replay scans. After positioning the robot to allow identification of the vessel of interest, this study proposes an automatic scanning mode implemented in an US scanner and exploiting the free command mode of the robot that allows controlling and moving it by a computer through a serial port. This study aimed to: 1) assess the automatic tracking trajectory and 3-D reconstruction with phantoms mimicking different vessel geometries with stenoses; and 2) evaluate the feasibility of this robotic imaging system for 3-D *in vivo* mapping of a normal femoral artery. For the first objective, 3D-US reconstructions were compared with the computer-aided design (CAD) files used for prototyping phantoms. For one specific phantom, comparison was also made with the 3D-CTA reconstruction, considered as the gold standard clinical examination. The *in vivo* feasibility was done to evaluate the performance efficacy of this robotic system under real clinical conditions.

## II. MATERIALS AND METHODS

### A. 3D-US Imaging Robotic System

As shown in Fig. 1, the prototype is composed of an industrial robot arm (F3 articulated robot, CRS Robotics Corporation, Burlington, ON, Canada), with six degrees of freedom, a force/torque sensor (ATI, Industrial Automation, Apex, NC, USA), and an open platform US scanner (Sonix Touch, Ultrasonix Medical Corporation, BC, Canada). The scanner was used as a control station for the 3D-US robotic system. B-mode images were acquired using the Ulterius platform provided by Ultrasonix. Each acquired image was associated with corresponding coordinates [i.e., position and orientation in the robot coordinate reference system (CRS)]. Images were captured at 10-MHz central frequency with a focus depth of 2–4 cm and an image depth of 5 cm to match optimum scanning conditions for 3-D vessel reconstructions reported earlier

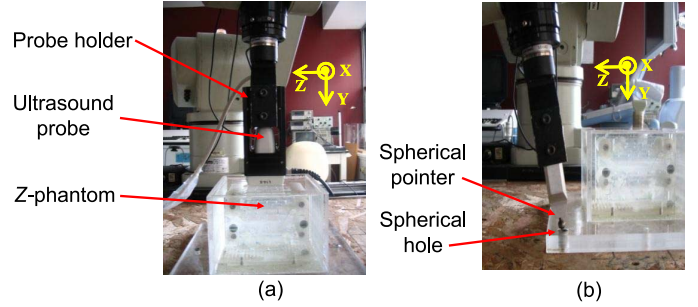


Fig. 2. Experimental setup of the probe calibration. (a) Setup to determine the position of wires in the US image. (b) Setup to determine the  $Z$ -phantom location in the robot CRS.

[15]. A 128-element linear array probe (L14-7, Ultrasonix) was used. The 3-D robotic system (i.e., robot arm motion and B-mode acquisition) was controlled using MATLAB (version 7.1, MathWorks Inc., Natick, MA, USA) installed on the US scanner. This F3 robot was also used by other teams for medical applications [16], [17].

### B. Probe Calibration

A calibration procedure based on a cross-wire phantom ( $Z$ -phantom) was used prior to 3D-US reconstruction, according to the method of [18]. The goal was to find the matrix transformation (orientation and translation) that converts 2-D coordinates of each pixel in the US image into 3-D coordinates in the robot CRS. Mathematically, this corresponds to solve the following equation:

$$\begin{pmatrix} x_k \\ y_k \\ z_k \\ 1 \end{pmatrix} = M_{\text{robot-base}}^{Z\text{-phantom}} \cdot M_{\text{US-probe}}^{\text{robot-base}} \cdot M_{\text{image}}^{\text{US-probe}} \cdot \begin{pmatrix} s_x \cdot u_k \\ s_y \cdot v_k \\ 0 \\ 1 \end{pmatrix} \quad (1)$$

where  $M_{\text{robot-base}}^{Z\text{-phantom}}$  is the unknown transformation matrix of the  $Z$ -phantom in the robot CRS,  $M_{\text{US-probe}}^{\text{robot-base}}$  is the known transformation matrix of the US probe in the robot CRS (the US probe is firmly fixed onto the robot arm with a custom-made probe holder), and  $M_{\text{image}}^{\text{US-probe}}$  represents the unknown transformation matrix of the US image with respect to the US probe 3-D position. The calibration setup (Fig. 2) used to find both unknown transformation matrices in (1) is explained in detail in [15]. A surgical polypropylene suture wire (8726 Prolene 6-0, Ethicon Inc., Piscataway, NJ, USA) of 0.07–0.099 mm in diameter was interwoven through holes to construct the  $Z$ -shaped patterns.

To determine  $M_{\text{image}}^{\text{US-probe}}$ , the US probe was attached to the robot arm with a probe holder and held over  $Z$ -phantom wires [Fig. 2(a)]. US image settings (i.e., beam focus depth, image depth, and zooming) were selected to represent US exams of lower limb peripheral arteries [19]. Each US image was manually segmented to determine the position of each wire. A Levenberg–Marquardt iterative algorithm was used to solve the calibration transforms, after locating the  $Z$ -phantom in the robot CRS by replacing the US probe by a spherical pointer [Fig. 2(b)] to determine  $M_{\text{robot-base}}^{Z\text{-phantom}}$  [15], [18], [20].

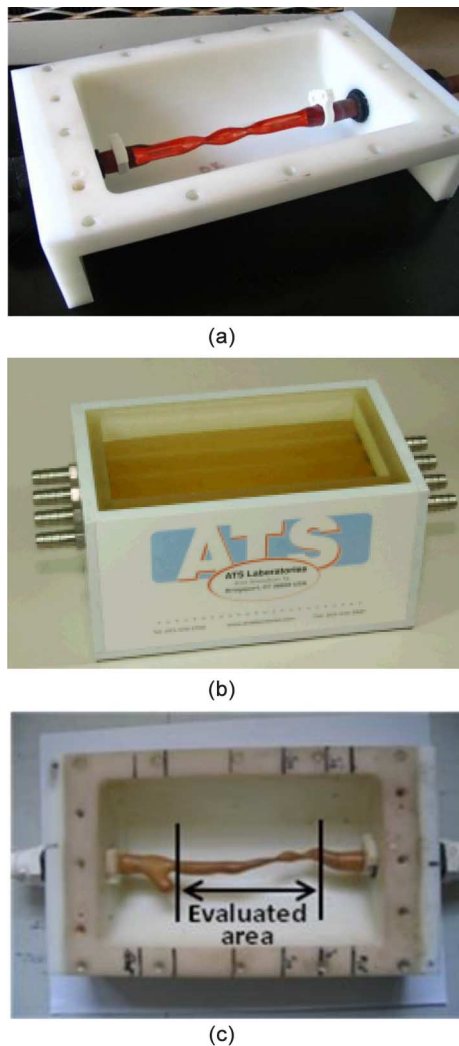


Fig. 3. Phantoms used to evaluate the 3D-US robotic system. (a) Phantom with double stenoses [21]. (b) Commercially available ATS phantom model #525 with four flow channels simulating superficial vessels, each channel containing one stenosis. (c) Iliac artery phantom with distributed severe stenoses [22]. Phantoms (a) and (c) are shown without the box top cover and the agar-mimicking tissue material used to fill the phantom.

### C. In Vitro Analysis of Simple Vessel Geometry Segments

To validate the automatic arterial trajectory tracking and 3D-US reconstruction, two phantoms with simple geometries were used. Both 3D-US reconstructions were compared with the CAD file used for prototyping the phantom geometry.

1) *Phantom #1 With Cosine-Shaped Double Stenoses*: The first phantom fabricated for this evaluation had a cross-sectional diameter of 7.9 mm for the nonobstructed lumen, and contained two adjacent axisymmetric stenoses [Fig. 3(a)]: one stenosis ( $S1$ ) with a 75%-area reduction and a second more severe stenosis ( $S2$ ) with 80%-area reduction. Both stenoses were cosine-shaped, had a length of 20 mm, and the distance between them was 24 mm. The gel surrounding the vessel lumen was made of 86% distilled water, 8% glycerol (# G-3730, ACP Chemical, Montreal, QC, Canada), and 3.5% agar (# A-9799, Sigma Chemical, St. Louis, MO, USA), which provided similar acoustic characteristics as human soft tissues (i.e., attenuation

and speed of sound) [21]. Once the gel was poured into the phantom container and was solidified, the sugar-based artery geometry inserted into connectors and attached by polyethylene clips at both ends of the container was melted with circulating hot water to create the vessel lumen.

2) *Phantom #2 With Abrupt Simple Stenoses*: The second phantom (model 525, ATS Laboratories, Knowlton St. Bridgeport, CT, USA) [Fig. 3(b)], designed for Doppler US flow imaging, contains four 8.0-mm diameter channels simulating superficial vessels with built-in stenoses at 0%, 50%, 75%, and 90% area reductions. To provide comparable results as phantom #1, we only used the channel with the 75% area reduction. The abrupt transition in the throat of the short stenosis provided another experimental condition to test the performance of the robotic system. The length of that stenosis was 4 mm.

### D. In Vitro Analysis of a Realistic Lower Limb Vessel Geometry

A third phantom mimicking a realistic lower limb iliac artery segment with distributed stenoses [Fig. 3(c)] was used to evaluate the tracking trajectory and 3D-US reconstruction. As for phantoms #1 and #2, the 3D-US reconstruction was compared with the corresponding CAD file. An additional evaluation aimed to compare results with 3D-CTA reconstruction, which is the gold standard clinical imaging technique for PAD diagnosis.

1) *Phantom #3 Mimicking an Iliac-Diseased Artery*: The phantom was constructed by considering a 3D-CTA reconstruction of a patient with PAD in the iliac artery. This mimicking artery contained multiple stenoses with two of them being more severe and labeled  $S1$  and  $S2$  with 97.3% and 98.3% area reductions, respectively. Dimensions measured on cross-sectional planes of the CAD file gave a value  $D = 6.5$  mm for the maximum diameter of the nondiseased vessel segment. Lengths measured between prestenotic and poststenotic maximum vessel diameters including stenoses  $S1$  and  $S2$  were  $L1 = 28.1$  mm and  $L2 = 14$  mm, and minimum diameters at stenoses were 1.4 mm for  $S1$  and 1.2 mm for  $S2$  (see later Fig. 8 for an illustration of  $L1$ ,  $L2$ ,  $S1$ , and  $S2$ ). The complete fabrication process, characteristics, and geometric accuracy of this phantom are available elsewhere [22]. A sugar-based lost material was also used for this phantom to create the vessel lumen. The sugar geometry was inserted in connectors and attached by polyethylene clips at the inlet and outlet of the phantom container before pouring the tissue mimicking material.

2) *Iliac Phantom #3 CTA Reconstruction*: To evaluate the accuracy of the 3D-US reconstruction according to clinical standards, a Somatom Sensation 64-slice scanner (Siemens, Erlangen, Germany) was used. The phantom was filled with contrast agent (Conray 43, Mallinckrodt Medical, Pointe-Claire, QC, Canada), then images were acquired with parameters as follow: 38.0-cm field of view for a-  $512 \times 512$  matrix size, 1.0-mm slice thickness, 217-mA current density, 120-kV peak voltage, and 0.6-mm reconstruction interval. The 3D-CTA reconstruction was realized with a maximum intensity projection (MIP) and a volume rendering, with the Visual software package (version 1.4, Object Research System, Montreal, QC, Canada). This representation was later transformed into

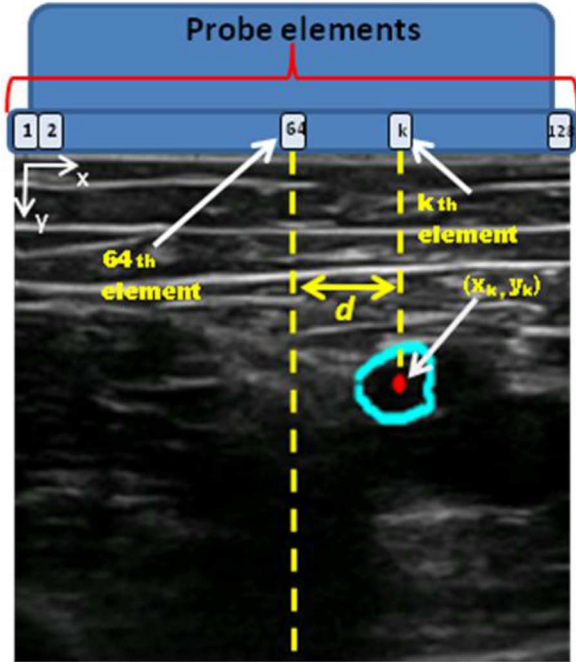


Fig. 4. Procedure used by the robot system to correct the trajectory of the artery with a B-mode image. The blue curve and red dot represent the segmented artery contour and its center of mass. Columns ( $x$ ) in the B-mode image represent probe elements and rows ( $y$ ) correspond to depth.  $d$  is the distance between the center of mass coordinate ( $x_k$ ) and the central element of the probe (64th) along the axis  $x$ .

a 3-D binary file that was converted into serial 3-D contours with SolidWorks (version 9.1, Dassault System, Vélizy-Villacoublay, France). The distance between each converted contour was 0.25 mm and the number of points in each contour was standardized to 100 with interpolation.

#### E. Automatic Tracking Trajectory and 3-D Reconstruction

The method described in this section was used *in vitro* and *in vivo* to evaluate the automatic tracking of the trajectory and 3-D reconstruction. *In vitro*, each phantom was fixed in the robot work space and then the US probe was placed over the phantom at one end of the vessel segment. Echographic gel was applied between the surface to be scanned and the US probe. One B-mode image was acquired and the vessel lumen segmented using a fast-marching method based on gray-level statistics and gradients adapted from [23]. This provided a contour of the artery lumen to start the automatic tracking process. Given that, each column in the acquired B-mode image (Fig. 4) was considered to represent the central probe element of the focused beam centered on the vessel. The coordinates ( $x_k$ ,  $y_k$ ) of the center of mass (red point) of the contour (blue curve) thus corresponded to the center of the arterial lumen. To ensure that the artery was at the center of the B-mode image to facilitate tracking of angulated vessels or to compensate for small motion artifacts (i.e., to avoid losing the vessel between successive images acquired along the  $z$ -axis), the distance  $d$  (Fig. 4) between the 64th element of the probe (central element) and the coordinate  $x_k$  of the center of mass was calculated as

$$d = (x_k - 64) \times T_e \quad (2)$$

where  $T_e$  is the element size of the probe (i.e., crystal size and pitch). After calculating the distance  $d$ , the MATLAB program sent a command to the robot to move the probe by a distance  $d$  to correct the trajectory, and maintain the artery at the center of the B-mode image. Then, the probe advanced by one step along the  $z$ -axis. The tracked trajectory length and step between each acquired image (fixed between 0.25 and 1 mm) could be set by the radiologist. In this study, a step of 0.25 mm *in vitro* and 1 mm *in vivo* were used.

The force/torque sensor, positioned between the US probe holder and the robot arm (Fig. 1), allowed maintaining a constant pressure during the scan by sending to the robot controller a function written in RAPL-3 (version 001b, CRS Robotics Corporation) before each new image acquisition. The RAPL-3 format is the programming language specific to this CRS robot. The process of image acquisition, segmentation, trajectory correction, and advancement of the probe by one step was applied until the robot completed its trajectory or was stopped by pushing a security button. Simultaneous 3D-US reconstruction was performed with acquired 2-D-segmented contours, for which  $x, y, z$  spatial positions were known. A real-time 3-D display on the US scanner screen was done using the MATLAB platform through the transformation matrix determined with the calibration procedure described earlier. To eliminate outliers and improve visual appearance of reconstructed 3-D images, the spatial filtering function “smooth” of MATLAB could be applied (span parameter = 5). Note that all quantitative measures of performance were computed on unsmoothed raw reconstructions.

#### F. Quantitative Analysis of Performance

For each 3-D reconstruction of phantoms, vessel cross-sectional areas and quantification of stenoses were compared with 3D-CAD files. In the specific case of the iliac phantom #3, comparisons were also made with the 3D-CTA reconstruction. For this purpose, a rigid registration was first performed with an iterative closest point (ICP) algorithm (MATLAB open source code ICP, version 1.4, by Per Bergström, March 7, 2007) to fit both US and CTA 3-D reconstructions.

1) *Lumen Cross-Sectional Areas*: Comparisons of cross-sectional areas between 3D-US reconstructions and 3D-CAD/CTA were realized along the  $z$ -axis with *Polyarea*, a polygon-specific function of MATLAB. This function computes the average number of pixels inside a closed contour. Cross-sectional areas of each contour were calculated and displayed along the  $z$ -axis.

2) *Quantification of Stenoses*: The severity of stenoses was defined as the percentage of reduction in diameter of the vessel compared to its larger diameter (diameter of reference) in a nondiseased segment. This measured  $S_A$ , where the subscript  $A$  indicates the modality (CAD, CTA, or US), is given by

$$S_A = 100 \times \left( \frac{D_r - D_i}{D_r} \right) \quad (3)$$

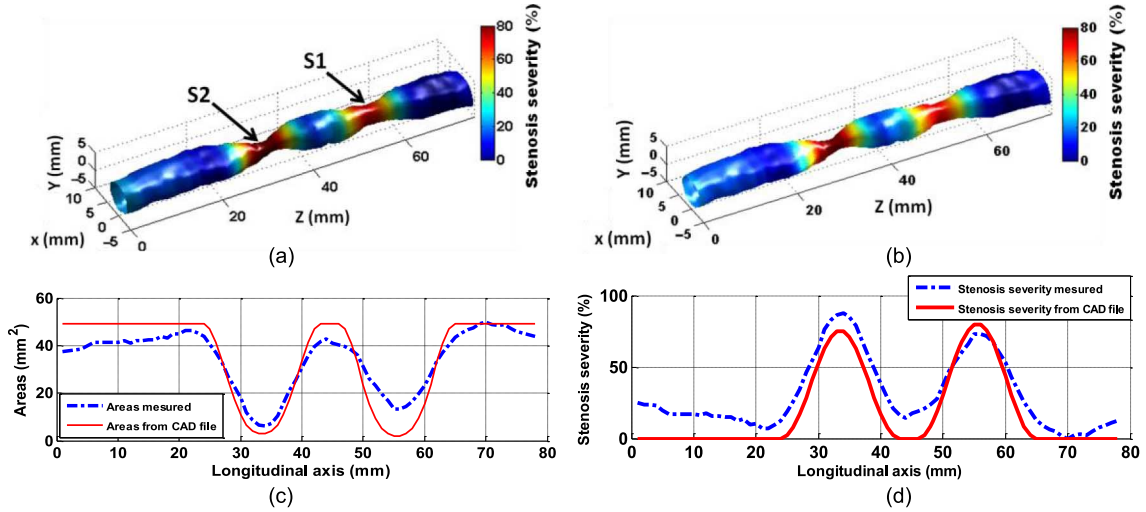


Fig. 5. Phantom #1 representing an artery with double stenoses. (a) 3D-US reconstruction of a segment including both stenoses (red color) from the raw data. (b) 3D-US reconstruction of the same segment with smoothing. (c) Cross-sectional areas plotted as a function of the longitudinal distance along the vessel. (d) Stenosis severity plotted as a function of the longitudinal distance. The color map represents the lumen area reduction in percent, where blue color corresponds to the largest area of the nondiseased artery.

where  $D_r$  is the reference diameter and  $D_i$  the diameter of the obstructed cross-sectional vessel lumen. For each reconstruction, percentages of stenosis were mapped along the  $z$ -axis. The length of stenoses was also compared between modalities.

3) *Hausdorff Distance*: This distance represents the worst-case fitting scenario between two methods. It is defined as the maximum distance of nearest points between two contours [24], [25]. The closest point distance associates each point on both curves to a point on the other curve, and the Hausdorff distance finds the largest distance between corresponding points, as indicated in (4). This performance measure was reported along the  $z$ -axis

$$Hd = \max \left( \max_i \{d(a_i, C_{US})\}, \max_j \{d(b_j, C_A)\} \right) \quad (4)$$

with

$$d(a_i, C_{US}) = \min_j \|b_j - a_i\| \quad (5)$$

where  $a_i$  and  $b_i$  represent  $x$  and  $y$  coordinates of a point on the set of points of both contours,  $C_{US} = \{b_1, b_2, \dots, b_n\}$  are points on the US contour, and  $C_A = \{a_1, a_2, \dots, a_n\}$  are points on the CTA or CAD contour ( $A = \text{CTA or CAD}$ ).

### G. In Vivo Feasibility Study

Given that major stenoses in PAD are localized in the femoropopliteal segment [2], [26], a pilot study was conducted on a 28-year-old healthy volunteer to evaluate the feasibility of the 3D-US robotic system to scan a superficial femoral artery. The protocol was approved by the institutional review board of the University of Montreal Hospital, and an informed consent was obtained.

The subject lay on his back in a decubitus position in the robot work space to allow access to the left leg. The radiologist positioned the US probe (L14-7, Ultrasonix) at one end of

the femoral artery segment to be scanned, in the same manner, and with the same equipment described above for *in vitro* studies. Scanning was done along the superficial femoral artery, from the bifurcation down to the distal femoral segment. Given that lower limb peripheral arteries are typically at a 3–8 cm depth range [19], we succeeded for this volunteer by choosing a 5-cm depth, a 2–4-cm focus beam depth (range where the arterial lumen was situated), and no zooming was selected. The scanning trajectory was followed with a cross-sectional B-mode view of the vessel longitudinal axis. Automatic tracking and 3-D reconstruction were in accordance with the method described in the *in vitro* study section II-E.

## III. RESULTS

### A. 3-D Representations of In Vitro Phantoms #1 and #2

To validate the automatic arterial trajectory tracking of the robotic system, 3-D reconstructions of *in vitro* vessel lumens were realized within the robot CRS using the Z-phantom calibration procedure. Fig. 5(a) describes the 3D-US representation of a segment of 78-mm length with double stenoses  $S1$  measured at 73% and  $S2$  at 87%. Fig. 5(b) shows the same 3-D representation with smoothing, whereas panels C–D give cross-sectional areas and percentages of stenosis along the  $z$ -axis. Cross-sectional areas of  $41.8 \pm 2.5 \text{ mm}^2$  were measured over the nondiseased segments; for the same regions, the mean area was  $49.0 \text{ mm}^2$  on the CAD file. As depicted in Fig. 5(d), the length of  $S1$  was 22 mm and that of  $S2$  was 23 mm. Compared with the CAD file, errors on stenosis lengths were 2 mm for  $S1$  and 3 mm for  $S2$ , whereas errors on stenosis severity were  $-2\%$  and  $+7\%$  for  $S1$  and  $S2$ , respectively.

Fig. 6(a) and (b) shows 3-D reconstructions of phantom #2 with a single tight stenosis segment of 60 mm in length, with and without smoothing. As shown in panel C, cross-sectional areas of the 3D-US reconstruction ( $50.0 \pm 1.9 \text{ mm}^2$ ) matched

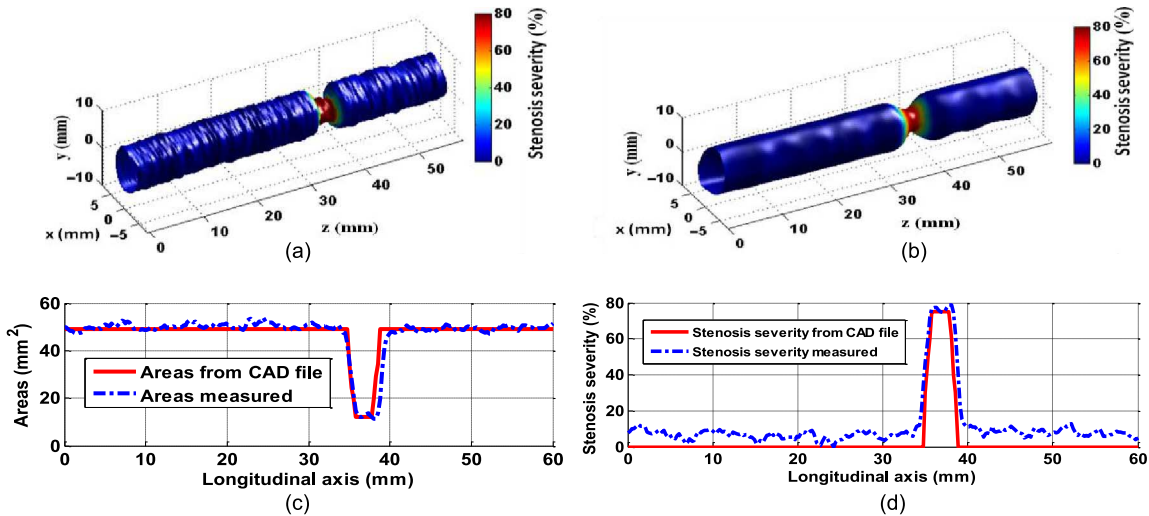


Fig. 6. ATS phantom #2. (a) 3D-US reconstruction of a segment including a stenosis of 75% (red color) from the raw data. (b) 3D-US reconstruction of the same segment with smoothing. (c) Cross-sectional areas plotted as a function of the longitudinal distance along the vessel. (d) Stenosis severity plotted as a function of the longitudinal distance. The color map represents the lumen area reduction in percent, where blue color corresponds to the largest area of the nondiseased artery.

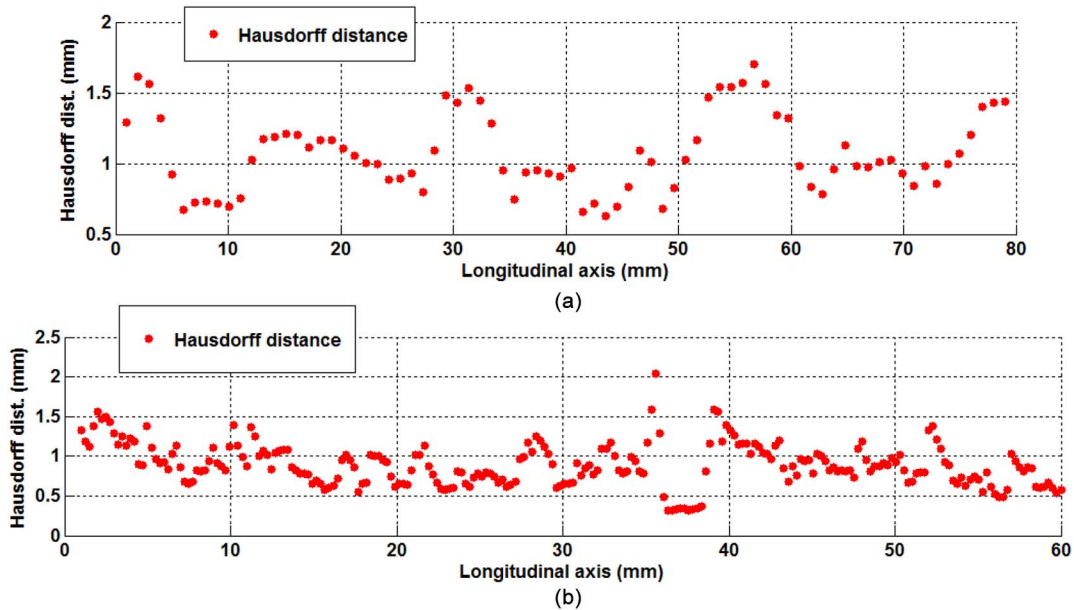


Fig. 7. Hausdorff distance plotted as a function of the longitudinal distance along the mimicking artery of phantoms (a) #1 and (b) #2; comparison between US and CAD.

well the CAD file (50.2 mm<sup>2</sup>) for nondiseased zones. Moreover, panel D illustrates the stenosis severity in percent along the  $z$ -axis with a maximum at 79%, and shows a stenosis length of 5.7 mm. Compared with the CAD file, error on the percentage of stenosis was +4% and error on the stenosis length was  $-1.7$  mm.

In Fig. 7, we report Hausdorff distances (4) between US and CAD contours along the  $z$ -axis for phantoms #1 and #2. For phantom #1 (panel A), it remained below 1.7 mm with maxima in the throat of both stenoses and at the beginning of the reconstruction, where larger errors in area and stenosis severity were also noticed in Fig. 5. Hausdorff distances were uniformly distributed and below typically 1.5 mm for phantom #2 (panel B), except in the tight stenosis where it reached a maximum slightly above 2 mm.

### B. 3-D Representations of In Vitro Phantom #3

The CAD file geometry of the iliac-diseased artery [Fig. 8(a)] shows the segment that was chosen to compare the 3D-CTA representation (panel B) with the 3D-US reconstruction (panel C) after rigid registration. Fig. 8(d) presents a superimposed representation of CTA and US scans in the same referential. A good agreement can be observed between both 3-D reconstructions. The 3D-CTA was scanned over a longer distance and its representation was thus 2.9 mm longer than the 3D-US display. The 3D-US geometry of Fig. 8(c) was reformatted in Fig. 9 to present the stenosis severity of the iliac-diseased artery without and with smoothing. The color map in both 3-D reconstructions is coded such that zero percent (blue color) corresponds to the largest area of the normal (nondiseased) segment of the artery.

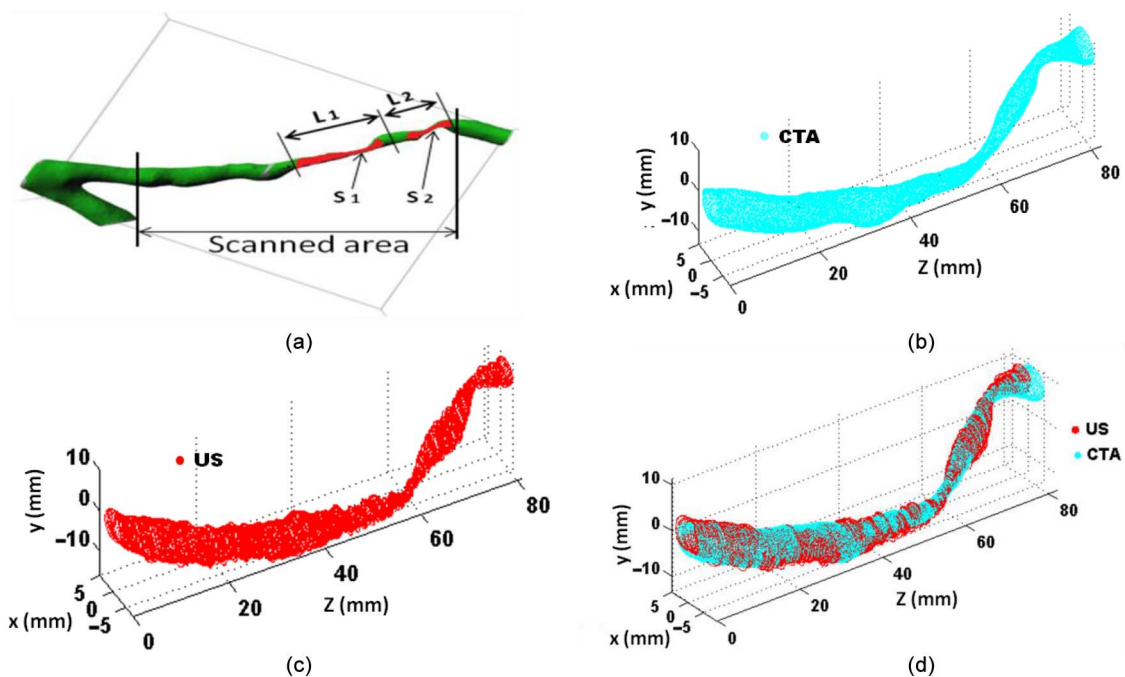


Fig. 8. 3-D representations of phantom #3 mimicking a diseased iliac artery. (a) 3D-CAD representation. (b) 3D-CTA reconstruction of the scanned segment of the artery depicted in (a). (c) 3D-US reconstruction of the same segment. (d) 3D-US and -CTA plotted in the same referential after 3D-US rigid registration.

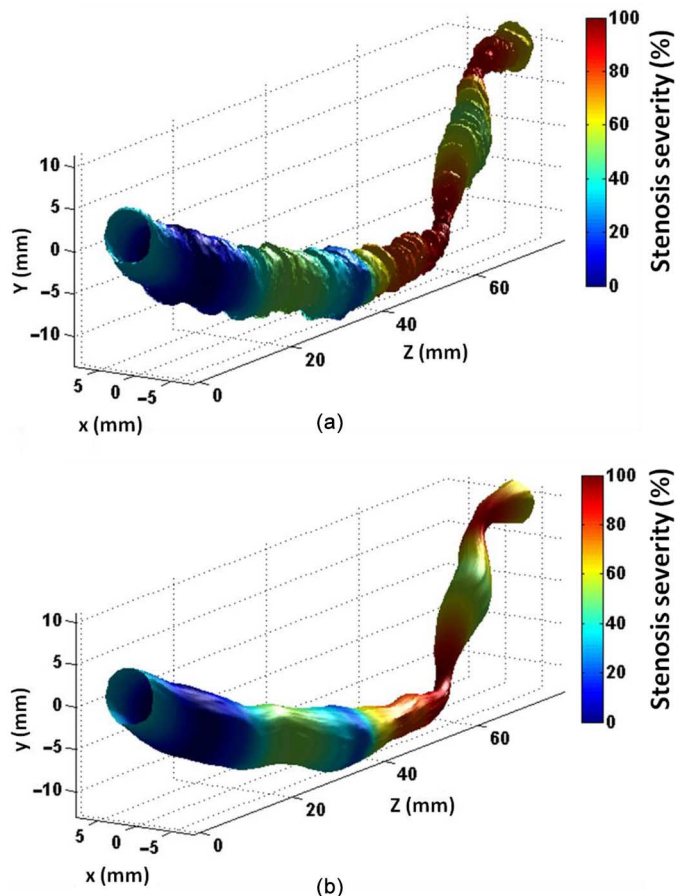


Fig. 9. 3D-US reconstruction of a segment of the phantom mimicking an iliac artery. (a) 3D-US reconstruction with raw data, (b) with smoothing data.

As illustrated in Fig. 10(a), the two curves show a good overlap between 3D-US and 3D-CTA cross-sectional areas. A good correspondence can also be observed in panel B for the stenosis severity. Errors in quantifying  $S1$  and  $S2$  were 3% and 7% between 3D-US and 3D-CTA. Table I reports the stenosis severity, stenosis lengths, and areas along with errors on CTA and US measures when compared with the CAD file geometry.

Finally, Fig. 11 reports Hausdorff distances (4) between both US and CTA contours along the  $z$ -axis. The mean Hausdorff distance along the iliac artery segment was  $0.97 \pm 0.46$  mm, which is within the limit of resolution of US. It remained uniformly distributed except toward the right end where it reached a maximum of 2.3 mm.

### C. In Vivo Feasibility Study

Fig. 12(a) and (b) (without and with smoothing) shows the performance of the robotic system to automatically track a presumably normal superficial femoral artery of a volunteer. The scan over a distance of 156 mm was conducted in 15 min; it included the vessel tracking, automatic segmentation, trajectory correction, and 3-D reconstruction. The color map is coded according to the lumen area, where blue corresponds to the largest area and red to the smallest area. Fig. 12(a) illustrates a 3D-US B-mode reconstruction of cross-sectional areas with the raw data along the  $z$ -axis; whereas Fig. 12(b) presents the same 3D-US reconstruction with smoothing. Fig. 13 presents the radius of each cross-section of the artery along the longitudinal downstream axis. To calculate the radius, we assumed that cross-sectional areas were circular. It can be observed that radii decreased progressively toward the knee, as expected for more peripheral lower limb arteries.

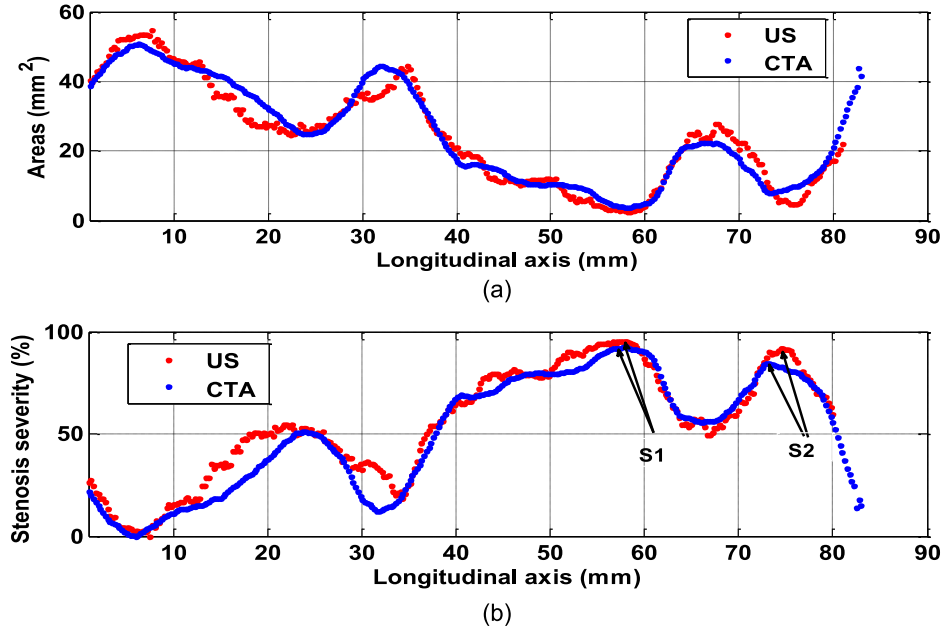


Fig. 10. (a) Cross-sectional area and (b) stenosis severity plotted as a function of the longitudinal distance along the iliac-mimicking vessel for 3D-CTA and -US reconstructions.

TABLE I  
SUMMARY OF *In Vitro* PERFORMANCE ASSESSMENTS FOR PHANTOM #3 MIMICKING AN ILIAC-DISEASED ARTERY

Stenoses	Stenosis severity (%)			Errors on stenosis severity (%) = reference - measured		
	CTA	US	CAD	CTA vs US	CAD vs CTA	CAD vs US
S1	92.5	95.5	97.3	-3.0	4.8	1.8
S2	84.5	91.5	98.3	-7.0	13.8	6.8
Stenoses	Stenosis length (mm)			Errors on length (%) = (reference-measured) / reference × 100		
	CTA	US	CAD	CTA vs US	CAD vs CTA	CAD vs US
S1	28.3	29.4	28.1	-4.2	-0.7	-4.9
S2	13.0	13.5	14.0	-3.8	7.1	3.5
Stenoses	Stenosis areas (mm <sup>2</sup> )			Errors on areas (%) = (reference-measured) / reference × 100		
	CTA	US	CAD	CTA vs US	CAD vs CTA	CAD vs US
S1	3.7	2.5	1.7	32.4	-117.6	-47.0
S2	7.8	4.5	0.95	42.3	-721.1	-373.6

#### IV. DISCUSSION

##### A. 3-D Vessel Reconstruction Analyses

In this study, simple geometries (single and double stenoses) were used to evaluate the automatic arterial trajectory tracking of the robotic system and corresponding 3D-US reconstructions. The robotic system allowed quantification of the severity and length of stenoses. In general, errors in area, in stenosis severity, and Hausdorff distances for phantoms #1 and #2

were higher within stenoses and at both ends. Explanations given below to elucidate those discrepancies between US and CAD in the case of phantom #3 also apply here. It was also observed when comparing results of Figs. 5 (phantom #1) and 6 (phantom #2) that better fits were obtained in the case of the latter commercial phantom. Errors in the fabrication process of phantom #1 (and #3) can explain this observation.

Next, a phantom mimicking a diseased iliac artery with multiple stenoses was used to compare the 3D-US reconstruction

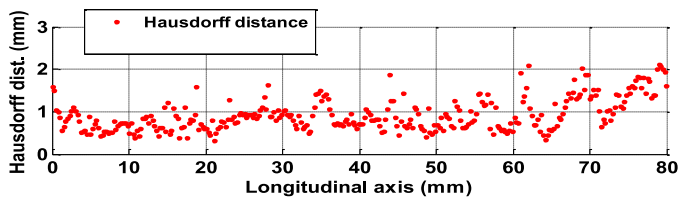


Fig. 11. Hausdorff distance plotted as a function of the longitudinal distance along the iliac artery (comparison between US and CTA).

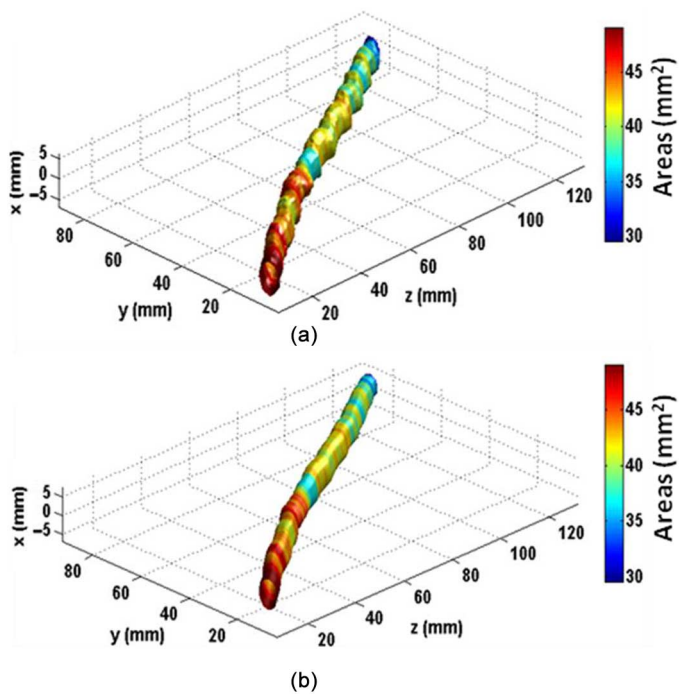


Fig. 12. 3D-US reconstruction of a segment of a superficial femoral artery of a normal volunteer. (a) 3D-US reconstruction with raw data and (b) with smoothing.

with CTA, which is the clinical gold standard. The latter investigation revealed comparable 3D-US and 3D-CTA maps. As noticed in Table I, both CTA and US overestimated the stenosis areas compared with the CAD geometry. This can be partially explained by the resolution of both methods [27], [28], and by CTA postprocessing (MIP, volume rendering, and smoothing filter) known to be user-dependent [29]. However, as introduced earlier, the most important source of errors was likely related to the fabrication process of the vascular phantom with reported errors up to 5.7% in diameter compared to the CAD file [22]. Indeed, in earlier reports [21], [22] (corresponding to phantoms #1 and #3 of this study), we compared microscopic histology slices of the constructed phantom with the CAD file and found errors between 1.4% in [21] and 5.7% in [22].

As reported in Figs. 7 and 11, 3D-US reconstructed cross-sectional lumen contours had higher Hausdorff distances with respect to CAD (Fig. 7) and CTA (Fig. 11) at the extremity. Larger errors at the extremity are likely due to shadowing caused by the high density polyethylene clip on the connector used for phantoms #1 and #3, which caused segmentation problems.

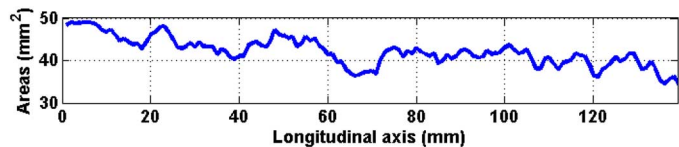


Fig. 13. Areas of the cross-sectional femoral artery as a function of downstream distances.

The feasibility of mapping *in vivo* a normal 3-D lower limb femoral artery was also tested under conditions approximating the clinical context. Besides evaluating lower limb arterial stenoses, the current robotic system may be of interest to grade the patency of lower limb bypass venous grafting [10]. Because regular follow-ups are required in this context, this would be a logical application of the robotic scanner to compete with the irradiating CTA or expensive MRA method.

*In vivo*, the robotic system has proven that it can compensate for small movements of the patient's leg with the tracking concept illustrated in Fig. 4. In view of providing a complementary noninvasive diagnostic technique, improvements in stenosis quantification would be possible using image compounding with acquisitions at different cross-sectional US views to improve the quality of B-mode images [30], [31]; this would also be feasible with plane wave imaging [32], [33]. Also, as mentioned above, the current implementation is limited because scanning *in vivo* a femoral artery over 156 mm required 15 min. The main reason for that was the use of three different computer languages to perform the vessel tracking, automatic segmentation, trajectory correction, and 3-D reconstruction. The B-mode image acquisition was done in C++ while the robot was controlled with the RAPL-3 programming language. The force/torque sensor allowing maintenance of a constant pressure on the scanned surface also used a function written in RAPL-3. Finally, the data management and synchronization of the different processing steps (i.e., acquired images, segmented contours, 3-D coordinates, and force/torque values) were controlled with MATLAB installed in the US Ultrasonix scanner.

Another limitation was noticed concerning the architecture and design of the robot arm. Indeed, beyond the maximum angle that a joint can reach, the robot reacted randomly. Therefore, the controlling software was designed to cut the power of the robotic scanner before such random behavior occurred, thus ensuring a safe scanning particularly in the case of future popliteal artery segment analysis, which runs behind the knee. To further remedy this potential issue, another robot has been specifically designed by our group for this application with strong compliance to safety concerns [34].

### B. Comparison With the Literature

A few studies performed with a tracking device attached to the US probe had similar objectives [35]–[37]. It is difficult to compare our results to these ones that were mainly based on electromagnetic (EM) freehand tracking, because authors have not evaluated the accuracy of their system against CTA, and focused mainly on demonstrating the technology's potential to monitor pathological changes in reconstructed vessels. The

progression of human atherosclerotic carotid plaques was monitored and analyzed with 3D-US systems controlled by a linear translation stage with a stepper motor [6], [9], [38]. Another 3D-US Flock-of-Bird EM system for measuring blood vessel geometries [35] allowed detecting a reduction in area of 48%. A study with a similar EM system found mean errors of  $-1.2\%$  to detect a 70% stenosis in carotid bifurcation phantoms [36]. Compared with CAD geometries, Janvier *et al.* found errors of 3.0% to detect an 80% stenosis and errors of  $-0.9\%$  to quantify a stenosis of 75% with a similar double stenosis phantom, as used in this study (phantom #1), and a robotic scanner [15]. Recently [39], with the same robotic system as in [15], they found errors of  $-11.8 \pm 6.1\%$  and  $-3.6 \pm 1.9\%$  to detect the 97.3% and 98.3% stenoses of the iliac phantom #3, respectively. The results of this study thus compare favorably with those of Janvier *et al.* [15], [39], conducted with a 3D-US robotic system with teach and replay modes. Also, maximum errors of 6.2% in area reduction were reported in [37] to quantify in-stent restenoses *in vitro* with an EM tracking device and phantom #1. Our results with that phantom gave errors with respect to CAD files of 2% and 7% to detect the 75% and 80% stenoses *S1* and *S2*, respectively.

In the above-mentioned studies, 3D-US freehand systems included positioning information from tracking devices that were used to locate each 2-D image in space and to reconstruct the sampled volume. Optical tracking uses emitting diode markers distributed on a rigid structure identified with cameras. For the current application, a limitation of such devices is the requirement of a constant line of sight between emitting diodes attached to the US probe and cameras. On the other hand, EM tracking measures the magnetic field between a receiver also attached to the US probe and a transmitter. Errors occur when metallic objects interfere with the magnetic field. Variable performances were reported depending on the scanning distance with respect to the static transmitter [13], [44]. Additionally, uneven volume sampling inevitably with 3D-US freehand systems may add uncertainty to the reconstruction. Consequently, these devices may not be optimum for lower limb vessel imaging where the detection and quantification of long and tortuous arterial segments requires a high precision. Robotic systems may thus be a superior strategy for this application. Finally, note that comparatively to our earlier teach/replay mode [14], [15], [39] where the system would continue the trajectory taught by the physician, even if the patient had moved, the current system adjusts its trajectory to small movements of the patient to perform a calibrated 3-D reconstruction. If this motion would become larger than a predefined distance fixed by the user (typically equal to the distance between two acquired images), the system was safely stopped. In this case, no 3-D reconstruction was done.

## V. CONCLUSION

As recently reported, the field of robotic US in medicine is still in its infancy [40] and only a few groups tackled the difficult problem of 3-D artery reconstructions [15], [34], [39], [41]–[43]. In this study, tracking vessel trajectory and 3-D reconstruction with an US imaging robotic

system were validated *in vitro* with vascular phantoms. 3D-US reconstructions showed good agreements with 3D-CTA in the case of a realistic diseased iliac artery phantom. We also verified the feasibility of this system *in vivo* in a normal volunteer and demonstrated that the system could compensate for potential small leg motions. Significant innovations with respect to our earlier contributions [14], [15], [39] were made. Namely, we eliminated the “teach” and “replay” mode, which could not compensate for leg movements between scans, by an automatic vessel tracking strategy requiring a single scan. Moreover, we replaced the B-mode video frame grabbing by an integrated software interfacing the robot controller with the Ulterius developing platform of the digital Ultrasonix scanner. The developed controlled software allowed triggering each digital image before segmenting the vessel, locating its center axis, making the robotic trajectory modification, and storing the resulting acquired image frame. At each iteration, if the force applied by the probe or the displacement became higher than prefixed values, the robot stopped, and its arm was moved away to assure a safe scanning. Further validations of this prototype would nevertheless be required. A clinical study on several patients with lower limb arterial diseases would be necessary to prove the applicability of the robotic system in the medical context. It may allow monitoring plaque progression and evaluating the impact of therapy with a modality that is safe, relatively inexpensive and not ionizing.

## REFERENCES

- [1] R. Collins *et al.*, “A systematic review of duplex ultrasound, magnetic resonance angiography and computed tomography angiography for the diagnosis and assessment of symptomatic, lower limb peripheral arterial disease,” *Health Technol. Assess.*, vol. 11, no. 20, pp. 1–202, May 2007.
- [2] L. Allard, G. Cloutier, L. G. Durand, G. O. Roederer, and Y. E. Langlois, “Limitations of ultrasonic duplex scanning for diagnosing lower limb arterial stenoses in the presence of adjacent segment disease,” *J. Vasc. Surg.*, vol. 19, no. 4, pp. 650–657, Apr. 1994.
- [3] J. Hung *et al.*, “3D echocardiography: A review of the current status and future directions,” *J. Amer. Soc. Echocardiogr.*, vol. 20, pp. 213–233, Mar. 2007.
- [4] E. Vicenzini *et al.*, “Three dimensional imaging of carotid arteries: Advantages and pitfalls of ultrasound investigations,” *Perspect. Med.*, vol. 1, no. 1–12, pp. 82–85, Sep. 2012.
- [5] A. Kurjak, G. Azumendi, W. Andonotopo, and A. Salihagic-Kadic, “Three- and four-dimensional ultrasonography for the structural and functional evaluation of the fetal face,” *Amer. J. Obstet. Gynecol.*, vol. 196, no. 1, pp. 16–28, Jan. 2007.
- [6] A. Delcker and H. C. Diener, “Quantification of atherosclerotic plaques in carotid arteries by three-dimensional ultrasound,” *Brit. J. Radiol.*, vol. 67, pp. 672–678, Jul. 1994.
- [7] A. Fenster, C. Blake, I. Gyacskov, A. Landry, and J. D. Spence, “3D ultrasound analysis of carotid plaque volume and surface morphology,” *Ultrasonics*, vol. 44, pp. e153–e157, Dec. 2006.
- [8] C. D. Ainsworth, C. C. Blake, A. Tamayo, V. Beletsky, A. Fenster, and J. D. Spence, “3D ultrasound measurement of change in carotid plaque volume,” *Stroke*, vol. 35, no. 9, pp. 1904–1909, Sep. 2005.
- [9] T. Wannarong *et al.*, “Progression of carotid plaque volume predicts cardiovascular events,” *Stroke*, vol. 44, no. 7, pp. 1859–1865, Jul. 2013.
- [10] D. F. Leotta *et al.*, “Measurement of anastomosis geometry in lower extremity bypass grafts with 3-D ultrasound imaging,” *Ultrasound Med. Biol.*, vol. 31, no. 10, pp. 1305–1315, Oct. 2005.
- [11] N. Pagoulatos, D. R. Haynor, and Y. Kim, “A fast calibration method for 3-D tracking of ultrasound images using a spatial localizer,” *Ultrasound Med. Biol.*, vol. 27, no. 9, pp. 1219–1229, Sep. 2001.

[12] D. M. Muratore and R. L. Galloway Jr., "Beam calibration without a phantom for creating a 3-D freehand ultrasound system," *Ultrasound Med. Biol.*, vol. 27, no. 11, pp. 1557–1566, Nov. 2001.

[13] D. D. Frantz, A. D. Wiles, S. E. Leis, and S. R. Kirsh, "Accuracy assessment protocols for electromagnetic tracking systems," *Phys. Med. Biol.*, vol. 48, pp. 2241–2251, 2003.

[14] M. A. Janvier *et al.*, "Performance evaluation of a medical robotic 3D-ultrasound imaging system," *Med. Image Anal.*, vol. 12, no. 3, pp. 275–290, Jun. 2008.

[15] M. A. Janvier, G. Soulez, L. Allard, and G. Cloutier, "Validation of 3D reconstructions of a mimicked femoral artery with an ultrasound imaging robotic system," *Med. Phys.*, vol. 37, no. 7, pp. 3868–3879, Jul. 2010.

[16] C. S. Tseng, C. C. Huang, and C. S. Chen, "Development of an image-guided robotic system for surgical positioning and drilling," *Robotica*, vol. 25, no. 3, pp. 375–383, May 2007.

[17] W. Zhouping, L. Gardi, D. B. Downey, and A. Fenster, "Oblique needle segmentation and tracking for 3D TRUS guided prostate brachytherapy," *Med. Phys.*, vol. 32, no. 9, pp. 2928–2941, Sep. 2005.

[18] F. Lindseth, G. A. Targen, T. Lango, and J. Bang, "Probe calibration for freehand 3-D ultrasound," *Ultrasound Med. Biol.*, vol. 29, no. 11, pp. 1607–1623, Nov. 2003.

[19] J. F. Polak, *Peripheral Vascular Sonography*, 2nd ed. Philadelphia, PA, USA: Lippincott Williams & Wilkins, 2004.

[20] L. Mercier, T. Lango, F. Lindseth, and L. D. Collins, "A review of calibration techniques for freehand 3-D ultrasound systems," *Ultrasound Med. Biol.*, vol. 31, no. 2, pp. 449–471, Feb. 2005.

[21] G. Cloutier *et al.*, "A multimodality vascular imaging phantom with fiducial markers visible in DSA, CTA, MRA, and ultrasound," *Med. Phys.*, vol. 31, no. 6, pp. 1424–1433, Jun. 2004.

[22] L. Allard, G. Soulez, B. Chayer, F. Treyve, Z. Qin, and G. Cloutier, "Multimodality vascular imaging phantoms: A new material for the fabrication of realistic 3D vessel geometries," *Med. Phys.*, vol. 36, no. 8, pp. 3758–3763, Aug. 2009.

[23] M. H. Roy Cardinal, G. Soulez, J. C. Tardif, J. Meunier, and G. Cloutier, "Fast-marching segmentation of three-dimensional intravascular ultrasound images: A pre- and post-intervention study," *Med. Phys.*, vol. 37, no. 7, pp. 3633–3647, Jul. 2010.

[24] D. P. Huttenlocher, G. A. Klanderman, and W. J. Rucklidge, "Comparing images using the Hausdorff distance," *IEEE Trans. Pattern Anal. Mach. Intell.*, vol. 15, no. 9, pp. 850–863, Sep. 1993.

[25] V. Chalana and Y. Kim, "A methodology for evaluation of boundary detection algorithms on medical images," *IEEE Trans. Med. Imag.*, vol. 16, no. 5, pp. 642–652, Oct. 1997.

[26] G. W. Taylor and A. R. Calo, "Atherosclerosis of arteries of lower limbs," *Brit. Med. J.*, vol. 1, pp. 507–510, Feb. 24, 1962.

[27] J. Nie, L. Lu, X. Gong, J. Nie, Q. Li, and M. Sun, "Determination of lower limb microvasculature by intrafemoral arterial injection using computed tomography-assisted angiography," *Aesthetic Plastic Surg.*, vol. 36, no. 6, pp. 1376–1381, Dec. 2012.

[28] O. V. Solberg *et al.*, "3D ultrasound reconstruction algorithms from analog and digital data," *Ultrasonics*, vol. 51, no. 4, pp. 405–419, May 2011.

[29] F. Rengier, T. F. Weber, F. L. Giesel, D. Bockler, H. U. Kauczor, and H. von Tengg-Kobligh, "Centerline analysis of aortic CT angiographic examinations: Benefits and limitations," *Amer. J. Roentgenol.*, vol. 192, no. 5, pp. W255–W263, May 2009.

[30] R. R. Entekin, B. A. Porter, H. H. Sillesen, A. D. Wong, P. L. Cooperberg, and C. H. Fix, "Real-time spatial compound imaging: Application to breast, vascular, and musculoskeletal ultrasound," *Semin. Ultrasound CT MRI*, vol. 22, no. 1, pp. 50–64, Feb. 2001.

[31] J. Y. Meuwly, J. P. Thiran, and F. Gudinchet, "Application of adaptive image processing technique to real-time spatial compound ultrasound imaging improves image quality," *Invest. Radiol.*, vol. 38, no. 5, pp. 257–262, May 2003.

[32] G. Montaldo, M. Tanter, J. Bercoff, N. Benech, and M. Fink, "Coherent plane-wave compounding for very high frame rate ultrasound and transient elastography," *IEEE Trans. Ultrason. Ferroelectr. Freq. Control*, vol. 56, no. 3, pp. 489–506, Mar. 2009.

[33] D. Garcia, L. Le Tarnec, S. Muth, E. Montagnon, J. Porée, and G. Cloutier, "Stolt's f-k migration for plane wave ultrasound imaging," *IEEE Trans. Ultrason. Ferroelectr. Freq. Control.*, vol. 60, no. 9, pp. 1853–1867, Sep. 2013.

[34] S. Lessard, P. Bigras, and I. Bonev, "A new medical parallel robot and its static balancing optimization," *J. Med. Devices*, vol. 1, pp. 272–278, Dec. 2007.

[35] T. C. Hodges, P. R. Detmer, D. H. Burns, K. W. Beach, and D. E. Strandless, "Ultrasonic three-dimensional reconstruction: In vitro and in vivo volume and area measurement," *Ultrasound Med. Biol.*, vol. 20, no. 8, pp. 719–729, 1994.

[36] D. C. Barratt, B. B. Ariff, K. N. Humphries, S. A. McG. Thom, and A. D. Hughes, "Reconstruction and quantification of the carotid artery bifurcation from 3-D ultrasound images," *IEEE Trans. Med. Imag.*, vol. 23, no. 5, pp. 567–583, May 2004.

[37] M. Lecart, M. H. Roy Cardinal, Z. Qin, G. Soulez, and G. Cloutier, "In vitro in-stent restenoses evaluated by 3D ultrasound," *Med. Phys.*, vol. 36, no. 2, pp. 513–522, Feb. 2009.

[38] A. Delcker, H. C. Diener, and H. Wilhelm, "Influence of vascular risk factors for atherosclerotic carotid artery plaque progression," *Stroke*, vol. 26, pp. 2016–2022, Nov. 1, 1995.

[39] M. A. Janvier, S. Merouche, L. Allard, G. Soulez, and G. Cloutier, "A 3D ultrasound imaging robotic system to detect and quantify lower limb arterial stenoses: In vivo feasibility," *Ultrasound Med. Biol.*, vol. 40, no. 1, pp. 232–243, Jan. 2014.

[40] A. M. Priester, S. Natarajan, and M. O. Culjat, "Robotic ultrasound systems in medicine," *IEEE Ultrason. Ferroelectr. Freq. Control*, vol. 60, no. 3, pp. 507–523, Mar. 2013.

[41] F. Pierrot *et al.*, "Hippocrate: A safe robot arm for medical applications with force feedback," *Med. Image Anal.*, vol. 3, no. 3, pp. 285–300, Sep. 1999.

[42] P. Abolmaesumi, S. E. Salcudean, Z. Wen-Hong, M. R. Sirospour, and S. P. DiMaio, "Image-guided control of a robot for medical ultrasound," *IEEE Trans. Rob. Autom.*, vol. 18, no. 1, pp. 11–23, Feb. 2002.

[43] R. Nakadate, J. Solis, A. Takanishi, E. Minagawa, M. Sugawara, and K. Niki, "Out-of-plane visual servoing method for tracking the carotid artery with a robot-assisted ultrasound diagnostic system," in *Proc. IEEE Int. Conf. Rob. Autom.*, 2011, pp. 5267–5272.

[44] W. Birkfellner *et al.*, "Systematic distortions in magnetic position digitizers," *Med. Phys.*, vol. 25, no. 11, pp. 2242–2248, Nov. 1998.



**Samir Merouche** received the B.Eng. degree in electronic engineering from the University El Hadj Lakhdar of Batna, Batna, Algeria, the Master's degree in biomedical engineering from the University of Lyon, Lyon, France, and the M.Sc. degree in biomedical engineering from the University of Montreal, Montreal, QC, Canada, in 1994, 2008, and 2013, respectively.

His research interests include applications of electronics in biomedical engineering and medical image processing.



**Louise Allard** received the Ph.D. degree in social sciences from the University of Montreal, Montreal, QC, Canada, in 1993.

After working as a scientist at a Quebec Government Health agency, she joined the Laboratory of Biorheology and Medical Ultrasonics, University of Montreal Hospital Research Center, Montreal, QC, Canada, to become a Research Coordinator, in 2002. She is also currently acting as the Technical Manager of the Experimental Imaging Platform with the University of Montreal Hospital

Research Center. Her research interests include quantitative ultrasound applied to red blood cell aggregation imaging and design of medical imaging vascular phantoms.



**Emmanuel Montagnon** was born in Nancy, France, in 1982. He received the B.Sc. degree in theoretical physics from the Université de Nantes, Nantes, France, and the Master's degree from the Université de Grenoble, Grenoble, France, in 2007. He completed the Ph.D. degree in biomedical engineering from the University of Montreal, Montreal, QC, Canada, in 2013, where he was conducting his research in the Laboratory of Biorheology and Medical Ultrasonics at the University of Montreal Hospital Research Center.

His research interests include dynamic ultrasound elastography and applications to breast cancer and deep vein thrombosis, shear wave scattering modeling, and plane wave imaging.



**Gilles Soulez** is a French citizen by birth. He completed his medical studies at the René Descartes University, Paris, France, and received the certification from the College of Interventional Radiology in 1990. He received the M.Sc. degree in clinical epidemiology at the University of Montreal in 2000. He became radiology board certified at the Royal College of Canada in 2010.

He is Professor of Radiology and Academic Chair with the Department of Radiology, Radio-Oncology and Nuclear Medicine, University of Montreal, Montreal, QC, Canada. He has funded the research Imaging Platform at the University of Montreal Hospital Research Center in 2000. He has authored 163 peer-reviewed papers and 26 book chapters. He is author or coauthor on 9 patents in the field of vascular and interventional radiology. His research interests include aneurysm endovascular repair, peripheral vascular disease, and advanced image guidance for interventional radiology procedures.

Dr. Soulez has been honored with several awards, including the Société Canadienne Française de Radiologie's Prize of Innovation in 2008, and the Award of Excellence and Innovation in Interventional Radiology at CIRSE 2013. He has also received multiple prizes for his publications, including from the Radiological Society of North America and the International Society of Endovascular Therapy.



**Pascal Bigras** received the B.Eng. and M.Eng. degrees in electrical engineering from the Department of Automated Manufacturing Engineering, École de Technologie Supérieure, University of Quebec, Montreal, QC, Canada, in 1991 and 1993, respectively, and the Ph.D. degree in automatic control from the École Polytechnique de Montréal, QC, Canada, in 1997.

He is currently an Associate Professor with the Department of Automated Manufacturing Engineering, École de Technologie Supérieure de Montréal. His research interests include nonlinear and robust control, robotics, and their applications.



**Guy Cloutier** (S'89–M'90–SM'07) received the B.Eng. degree in electrical engineering at the Université du Québec à Trois-Rivières, and the M.Sc. and Ph.D. degrees in biomedical engineering at the École Polytechnique of Montreal in 1984, 1986, and 1990, respectively.

From 1990 to 1992, he was a Postdoctoral Fellow with The Pennsylvania State University, State College, PA, USA. He is the Director of the Laboratory of Biorheology and Medical Ultrasonics, University of Montreal Hospital Research Center, QC, Canada ([www.lbum-crchum.com](http://www.lbum-crchum.com)), Professor and Director of Research with the Department of Radiology, Radio-oncology, and Nuclear Medicine, and Member with the Institute of Biomedical Engineering, University of Montreal. He has authored more than 170 peer-reviewed articles in these fields, holds 12 patents, and licensed two technologies. His research interests include quantitative ultrasound imaging of red blood cell aggregation, quasi-static and dynamic ultrasound elastography of atherosclerotic plaques, vascular aneurysms, deep vein thrombi, breast cancers and liver steatosis, 3D morphologic and hemodynamic assessment of lower limb arterial stenoses, development of multiphysics imaging methods, and mathematical and biomechanical modeling.

Dr. Cloutier is an Associate Editor for the IEEE TRANSACTIONS ON ULTRASONICS, FERROELECTRIC AND FREQUENCY CONTROL, Invited Associate Editor for *Medical Physics*, Member of the Editorial Board of *Current Medical Imaging Reviews*, and was a Member of the international advisory Editorial Board of *Ultrasound in Medicine and Biology* for 15 years. He was the recipient of the National Scientist award of the Fonds de la Recherche en Santé du Québec (2004–2009)